



2023

Does tssH deletion in *Paraburkholderia bonniea* affect its symbiosis with *Dictyostellum discoideum*?

Anna Chen
Colby College

Follow this and additional works at: <https://digitalcommons.colby.edu/honorstheses>



Part of the [Bioinformatics Commons](#)

Colby College theses are protected by copyright. They may be viewed or downloaded from this site for the purposes of research and scholarship. Reproduction or distribution for commercial purposes is prohibited without written permission of the author.

Recommended Citation

Chen, Anna, "Does tssH deletion in *Paraburkholderia bonniea* affect its symbiosis with *Dictyostellum discoideum*?" (2023). *Honors Theses*. Paper 1398.
<https://digitalcommons.colby.edu/honorstheses/1398>

This Honors Thesis (Open Access) is brought to you for free and open access by the Student Research at Digital Commons @ Colby. It has been accepted for inclusion in Honors Theses by an authorized administrator of Digital Commons @ Colby.

Does *tssH* deletion in *Paraburkholderia bonniea* affect its symbiosis with
Dictyostelium discoideum?

Anna Chen

Computational Biology Honors Thesis 2023

Department of Biology

Colby College

**Does tssH deletion in *Paraburkholderia bonniea* affect its symbiosis with
Dictyostelium discoideum?**

An Honors Thesis

Presented to
The Faculty of the Department of Biology
Colby College

In partial fulfillment of the requirements for the
Degree of Bachelor of Arts with Honors

Anna Chen
Waterville, Maine

Examined and Approved on May 8, 2023

Advisor Suegene Noh  _____

Reader Lynn Hannum  _____

Reader Ron Peck  _____

Abstract:

Paraburkholderia are amoeba resistant, gram negative bacteria that form facultative symbiotic relationships with *D. discoideum*, a soil dwelling amoeba host. Three species of *Paraburkholderia*, *P. agricolaris*, *P. hayleyella*, and *P. bonniea* are able to persistently infect nonnative, or symbiont free, *D. discoideum*. These three species share a type III secretion system (T3SS) and type VI secretion system (T6SS) that is absent in other close relatives. We hypothesized that the ability to persistently infect *D. discoideum* may be partially attributed to the T3SS and T6SS shared across the three species of *Paraburkholderia*.

The goal was to test the phenotypic effect of a *P. bonniea tssH* ATPase gene knockout within the shared T6SS complex. We hypothesized that the ability of the mutant $\Delta tssH$ to infect and influence host fitness compared to the wild type would be significantly reduced. To compare the wildtype versus mutant variants of *P. bonniea*, we performed two assays. In each, *D. discoideum* hosts were paired with wildtype *P. bonniea* bb859 and bb433 strains, along with their respective mutant strains. These assays assessed differences between mutant and wildtype strains in changes in host fitness as infection prevalence increases and how host fitness was affected. We also generated and analyzed RNA sequencing data to understand the molecular impact of T6SS perturbation in this amoeba-bacteria symbiosis.

Although some phenotypic differences were observed between $\Delta tssH$ variants with the *tssH*-ATPase gene knockout within the T6SS and wildtype *P. bonniea* infected

D. discoideum hosts, their impact on how host fitness changed as infection prevalence increased was not different between the $\Delta tssH$ mutant and wildtype. This observation was also reflected in our RNA-sequencing data, where there were no statistically-significant differentially expressed genes between them. However, significant differences were observed between the variants during horizontal transmission, where infection was spread from host to host. Thus, the T6SS may be closely involved with virulence after the bacteria has entered the cell, rather than immediately upon encountering the host.

Acknowledgements:

Special thanks to Dr. Suegene Noh for which this research would not be possible otherwise. The innumerable number of hours we spent together on the weekends and over the summer, and your untiring support and feedback kept me driven throughout this project. Thank you to my lab members Tom Mu '23 and Abby Folsom '24 for their work in supporting my experiment, and other members of the lab (Kayla Dixon '23 and Lily Moy '23) for general support and camaraderie. Thank you to Dr. Ron Peck, Rachel Covitz '22, and Sadie Kuhn '22 in their work for generating the mutant *P. bonniea*. I also thank Dr. Lynn Hannum and Dr. Ron Peck for being on my advisory committee and providing invaluable feedback and support. Thank you to my roommates and friends for their moral support and encouragement throughout this thesis. This project was supported by the National Institutes of Health and its National Institute of General Medical Sciences by an Institutional Development Award (IDeA) under Grant Number P20GM103423 (subaward to S. Noh).

Table of Contents

Abstract:	3
Acknowledgements:	5
Table of Contents	5
Introduction:	7
Methods:	11
Bacteria and amoeba samples:	11
Δ tssH <i>P. bonniea</i> knockout generation:	11
Phenotype analysis	12
Fitness assay:	12
Horizontal transmission assay:	13
Statistical methods:	16
RNA-seq Analysis	16
RNA collection:	16
Differential expression analysis:	18
Results:	20
Host Fitness:	20
Horizontal Transmission:	21
RNA-seq	23
Δ tssH mutant vs wildtype:	23
Time series:	24
Discussion:	35
Conclusion:	40
Citations:	41

Introduction:

Dictyostelium discoideum is a soil-dwelling social amoeba commonly used to model host-pathogen interactions with both single-cellular and multicellular life stages (Bozzaro and Eichinger, 2011; Dunn et al., 2019; Skriwan et al., 2002). Thus, *D. discoideum* is useful as a host for understanding the mechanisms of pathogenesis in a bacterial infection (Bozzaro and Eichinger, 2011; Solomon and Isberg, 2000; Steinert, 2011, Thewes et al., 2016). *D. discoideum* are resistant to or eliminate most internal pathogens during both life stages through innate immune mechanisms and consumes them through phagocytosis (Chen et al., 2007; Farinholt et al., 2019; Peracino et al., 2013; Sillo et al., 2008; Vines and King, 2019; Walk et al., 2011). However, *Paraburkholderia* are amoeba resistant, gram negative bacteria that are uniquely able to form facultative symbiotic relationships with *D. discoideum* (Haselkorn et al., 2019). The intracellular infection persists through *D. discoideum*'s social cycle and transmits to later generations. Approximately a third of wild isolates of *D. discoideum* have been stably associated with several bacteria species, including *Paraburkholderia* (Brock et al., 2011; DiSalvo et al., 2015).

D. discoideum has a unique multistage life cycle. When food bacteria is plentiful, the single-cell amoeba is in its vegetative state and divides by binary fission. After the food bacteria are depleted, *D. discoideum* aggregates into its multicellular slug stage. The multicellular slug is able to migrate to a new location, where it differentiates into a fruiting body. The fruiting body is composed of two components - the stalk and the sorus, which contains spores that will germinate into vegetative amoeba (Kessin, 2001).

During the social stage, infected *D. discoideum* persistently carries both edible (food) and inedible (symbiotic) bacteria, ensuring a food source in the new environment (DiSalvo et al., 2015). When infected, the amoeba slug migrates shorter distances with less food bacteria and produces fewer spores and fruiting bodies for dispersion into the next generational growth cycle (Brock et al., 2011; DiSalvo et al., 2015; Shu et al., 2018).

Three species of *Paraburkholderia*, *P. agricolaris*, *P. hayleyella*, and *P. bonniea* are able to persistently infect nonnative, or symbiont free, *D. discoideum* (DiSalvo et al., 2015). When *D. discoideum* are infected with *Paraburkholderia* symbionts, host fitness is generally reduced (Brock et al., 2011; DiSalvo et al., 2015). Infection outcomes of *D. discoideum* hosts differ depending on the species and strain of the *Paraburkholderia* it is exposed to. Generally, *P. hayleyella* infections are characterized as the most detrimental to spore productivity, then *P. agricolaris*. *P. bonniea* appears to be the most mild, reducing spore productivity much less drastically than the other two species (Brock et al., 2020; Khojandi et. al, 2019; Miller et.al, 2020). These three species share a type III secretion system (T3SS) and type VI secretion system (T6SS) that is absent in other close relatives (Noh et al., 2022). We hypothesize that the ability of *Paraburkholderia* to persistently infect *D. discoideum* may be partially attributed to the T3SS and T6SS shared across the three species of *Paraburkholderia*.

T3SSs and T6SSs are critical virulence determinants in several Gram-negative pathogens (Chen et al., 2011; Lennings, 2018). The T6SS is used by bacteria to

deliver bacterial effectors directly into eukaryotic host cell cytosols or other bacteria (Francis et al., 2002; Taylor et al., 2018). The T6SS comprises 13 conserved and essential components named TssA to TssM (Cascales and Cambillau, 2012; Zoued et al., 2014). We will be primarily focusing on the TssH component in T6SS-5 operons, which have been shown to be functionally linked to virulence in *B. pseudomallei* and *B. thailandensis*, with the adjacent T3SS-3 operons regulating the expression of T6SS-5 (Chen et al., 2011; Schwarz et al., 2010; Shalom et al., 2007; Sun et al., 2010). The T6SS is a complex contractile injection system that allows bacteria to inject proteins, toxins and bacterial effectors directly into host cell membranes or cytoplasm. The secretion nanomachine mechanism contracts and extends through the bacterial double membrane where substrates are conveyed from the bacterial cytoplasm into the host cell (Alteri and Mobley, 2016; Gallique et al., 2017). This nanomachine consists of three main complexes: proteins in the inner membrane that are T4SS component-like, the baseplate complex, and the contractile sheath tail complex, which are formed by components evolutionarily related to contractile bacteriophage tails (Chen et al., 2011; Navarro-Garcia, 2019). The baseplate serves as a platform for contractile tail elongation, which in turn propels effectors across membranes. Finally, the TssH ATPase (ClpV) is recruited to the contracted sheath to recycle the sheath and other T6SS components (Förster et al., 2014; Gallique et al., 2017).

In *B. pseudomallei*, several macrophage-inducible genes were theorized to contribute to virulence, including three genes (*tssH*, *tssI* and *tssM*) within T6SS-5 (Shalom et al., 2007). Looking at the *tssH* gene specifically, it is part of an ATP binding cassette (ABC)

system, which are generally responsible for transmembrane import and export of a wide variety of molecules. ABC transporters have a highly conserved ATPase domain (nucleotide-binding domain) which mediates ATP binding and hydrolysis to provide energy for the substrate transport and increased uptake of various nutrients (Harland et al., 2007; Pietrosiuk et al., 2011). ABC systems are proposed to be associated with infection through virulence factors and mechanisms like haemolysin-type macromolecules expressed in the host during infection, lipopolysaccharides from the outer bacterial membrane, and capsule polysaccharides in both *B. mallei* and *B. pseudomallei* (Deshazer et al., 1999; Deshazer et al., 2001; Garmory and Titball, 2004; Harland et al., 2007; Reckseidler-Zenteno et al, 2005).

Thus, we aim to test the phenotypic and transcriptional effect of a *P. bonniea tssH* ATPase gene knockout within the type VI complex. We hypothesize that the ability of the *P. bonniea ΔtssH* ATPase knockout mutant to infect and influence host fitness compared to the wild type will be significantly reduced. Additionally, we predict that rates of horizontal transmission, which are bacteria that are transmitted from host to host, rather than from mother to daughter cells, will be decreased. We also generate and analyze RNA sequencing data to understand the molecular impact of type VI secretion perturbation in this amoeba-bacteria symbiosis. Gene deletions of the *tssH* gene were constructed in two *P. bonniea* strains - bb433 and bb859. In the host fitness and horizontal transmission assays, we use *P. bonniea* strains bb433 and bb859, while the RNA sequencing experiment uses only *P. bonniea* strain bb433.

Methods:

Bacteria and amoeba samples:

We cultured *P. bonniea* and *Klebsiella pneumoniae* food bacteria on SM/5 plates [2 g glucose, 2 g BactoPeptone (Oxoid), 2 g yeast extract (Oxoid), 0.2 g MgCl₂, 1.9 g KH₂PO₄, 1 g K₂HPO₄ and 15 g agar per liter]. We used two pairs of RFP labeled *P. bonniea* strains: bb433 Δ *tssH* with bb433 wildtype (WT), and bb859 Δ *tssH* with bb859 WT. We grew *D. discoideum* on SM/5 plates with 2×10^5 spores and *K. pneumoniae* (250 μ L at 1.5 OD_{600 nm}) in a 21 °C incubator for all assays. Two nonnative *D. discoideum* hosts (not associated with *Paraburkholderia* in the wild) were used for all experiments: QS4 and QS864 as biological replicates. Both *D. discoideum* strains were isolated from Mt. Lake Biological Station in Virginia, USA.

Δ tssH P. bonniea knockout generation:

To generate the mutant *P. bonniea* bb433 and bb859 with a knockout *tssH* ATPase gene, we conducted Gateway-compatible allelic exchange using homologous recombination. A two-step polymerase chain reaction (PCR) was performed to construct a recombinant plasmid to allow an in-frame deletion of codons 8-957 (2850 bp) of the 966-codon open reading frame on Geneious Prime ver 2020.2.5 (<https://www.geneious.com>). In the first step, PCRs were carried out with primer pairs RP966 (ACAAAAAAGCAGGCTgggcaacgatatcgagcagatc - lowercase letters bind to genomic DNA template) with RP967 (TCCGGTCGCTTTTGTGGCcttgaggctgagctgaatcatg) and RP968 (gccacaaaagcgaccgga) and RP969 (TACAAGAAAGCTGGGTgtcgaagtgctcgccatag)

using *P. bonniea* (bb859) genomic DNA as template. These PCR products were then used as template in the second-step PCR with primers RP956 (GGGGACAAGTTTGTACAAAAAAGCAGGCT) and RP957 (GGGGACCACTTTGTACAAGAAAGCTGGGT) to generate the deletion gene and add *attB1* and *attB2* sites. This product was then used in a Gateway cloning reaction with pDONRPEX18Tp-Scel-pheS (Fazli, 2015) to generate pRFP505.

pRFP505 was introduced into *P. bonniea* strains bb433 and bb859 by electroporation. Genomic integrants were confirmed by PCR and the strains were then transformed with pDAI-Scel-pheS (Fazli, 2015) and recombinants were screened by PCR.

To verify the successful deletion of the *tssH* ATPase in *P. bonniea* bb433 and bb859, Oxford Nanopore sequencing was performed at Seqcenter (Pittsburgh, PA). A BLAST library of all sequenced reads was constructed using BLAST ver 2.11.0+ (Camacho et al., 2019). Within the library, we queried for the knockout gene. No matches of the full nucleotide sequence were identified, indicating a successful deletion. To further confirm the deletion, the starting and ending sequence of the *tssH* gene were connected to each other, indicating a successful gene deletion.

Phenotype analysis

Fitness assay:

To measure host fitness between *P. bonniea* $\Delta tssH$ mutants and *P. bonniea* WT samples using spore productivity, triplicate *D. discoideum* infections were set up at 0.3 MOI, 1.5

MOI, and 7.5 MOI *P.bonniea* to 2×10^5 *D. discoideum* spores. We plate the same number of bacterial cells per plate, so the percentage indicated the percent of *P. bonniea* amongst food bacteria. For each *P. bonniea* strain $\Delta tssH$ mutant and wildtype pair, we conducted the experiment with two different hosts as biological replicates. We incubated the *D. discoideum* cultures for 5-7 days until they formed fruiting bodies. Spore samples were harvested for infection prevalence and spore count assays. Total spore counts were quantified using a light microscope and hemocytometer at a 200x dilution. To examine the relationship between host fitness and infection, infection prevalence (percent of RFP+ infected spores in a sample of 100,000 cells) flow cytometry was used to run a sample of spores on a Sony SH800 Cell Sorter (Sony Biotechnology, San Jose, CA). The FCS files were imported into FlowJo v10.8.1 for analysis (BD Life Sciences). We gated the spores, then subsetted the dyed cells from the negative using the negative control and highest MOI samples.

Horizontal transmission assay:

To measure horizontal transmission, we compared symbiont transmission to initial symbiont infection prevalence. Pre-infected amoebas were exposed to uninfected amoebas during the social stage, and horizontal transmission was measured as the percentage of newly infected spores. The pre-infected *D. discoideum* infections were prepared onto SM/5 plates at 0.3 MOI, 1.5 MOI, and 7.5 MOI RFP-labeled *P.bonniea* to 2×10^5 *D. discoideum* spores. After fruiting bodies formed, we collected the infected spores. The infected spores and fresh, uninfected spores were separately plated onto fresh SM/5 plates at densities of 2×10^5 and 1×10^5 spores per plate with food bacteria.

36 hours post incubation, amoebae in log-phase growth were collected from SM/5 plates. The uninfected amoebas were dyed with CellTracker™ green CMFDA Dye (Invitrogen) dissolved in DMSO. Pre-infected amoebas carrying RFP+ *P. bonniea* were exposed to DMSO only. Both sets were washed and incubated together. Then, the uninfected dyed amoebas were combined with the infected RFP+ amoebas at - 1:0 (dye-only negative control), 0:1 (infected only positive control), and 1:1 (mixed) ratios. These mixes were spread onto nitrocellulose filters (Millipore) moistened with KK2 in replicates of three. The filters were left to aggregate and turn into fruiting bodies, which we collected 5-7 days later. We conducted these experiments for two biological host replicates for each *P. bonniea* strain $\Delta tssH$ mutant and wildtype pair.

The spore samples were run through flow cytometry on a Sony SH800 Cell Sorter to quantify infection prevalence, which is a combination of *P. bonniea*'s ability to infect *D. discoideum* and horizontally transmit (Sony Biotechnology, San Jose, CA). In FlowJo v10.8.1, spores were gated, then dyed cells from the negative control (Figure 1a), and then the infected cells from the highest MOI sample (Figure 1b). Horizontal transmission was detected by measuring the percent of spores which had a co-occurrence of the green-labeled dye and red-labeled infection within one spore (Figure 1c). The spores in this population were previously uninfected amoebas but that were now positive for symbiont infection.

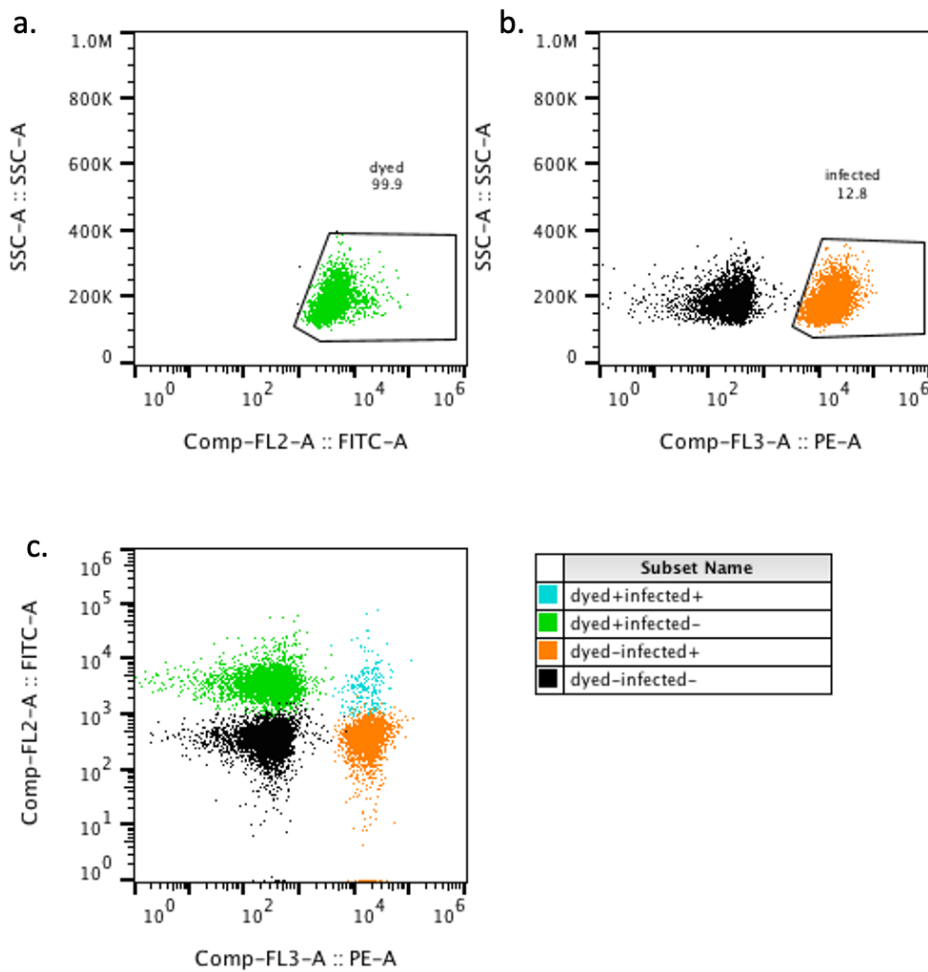


Figure 1: Sample results of the horizontal transmission assay when run through flow cytometry. A. The green population indicates spores that were dyed with CellTracker™ green CMFDA Dye. These spores were initially uninfected. B. Infected cells are gated (orange) from uninfected cells (black) through the detection of red fluorescence from the RFP labeled *P. bonniea*. C. The horizontal transmitted population are gated in blue as the population with both green fluorescence (initially uninfected) and red fluorescence (infected with RFP labeled *P. bonniea*).

Statistical methods:

Statistical analyses were performed using R v.4.2.2 and with packages ggplot2 v.3.5.5 (Wickham, 2016) and car v.3.0-12 (Fox and Weisberg, 2019). For both host fitness and symbiont transmission, we separately fit linear models with mixed effects on *P. bonniea* 433 and 859. Infection prevalence from flow cytometry data was coded as a continuous predictor, and the linear model accounted for experiment date and host strain as random effects. We separately tested how percent spores (relative percent of spores produced) were affected by symbiont treatment ($\Delta tssH$ or WT) while controlling for host strain. We started by fitting a complex model, and then a reduced model with non-significant terms removed. If no significant differences were identified between the two models using a chi-squared test, the simpler model was applied. To test for difference in infection prevalence, a nonparametric Wilcoxon test was conducted between $\Delta tssH$ mutant and wildtype variants. Residuals were evaluated on the final model to ensure model assumptions were held.

RNA-seq Analysis

RNA collection:

We aimed to detect gene expression changes between host transcripts upon infection by *P. bonniea* $\Delta tssH$ mutants and *P. bonniea* WT samples. To accomplish this, two *D. discoideum* strains or clones, QS4 and QS864, were infected by *P. bonniea* 433 $\Delta tssH$ or *P. bonniea* 433 WT and RNA was collected at 90 minutes post infection (mpi) and at 360 mpi. Two days prior to the experiment day, we prepared uninfected *D. discoideum* and positive control samples. Positive control samples acted as longer-term infections

(2250 mpi) and were infected with bb433 $\Delta tssH$ at 60 MOI (2.5%) and bb433 WT at 24 MOI (1%). The night prior to the experiment day, 0.5 OD₆₀₀ *K. pneumoniae*, 2 OD₆₀₀ *P. bonniea* solutions were prepared. Approximately 36 hours after the initial plating, amoebae were collected in log-phase growth. Approximately 12 hours after initial plating, *P. bonniea* were collected in log-phase growth. With these cells, we prepared four uninfected controls, two positive controls each for the *P. bonniea* 433 $\Delta tssH$ /433 pairs, and four replicates of bb433 $\Delta tssH$ at MOI 60, and bb433 WT at MOI 24. To conduct the time series, negative controls, positive controls, and 2 of each infection were collected 90 minutes post-infection. An additional 2 samples of each infection were collected at 360 minutes post-infection.

Genomic RNA was preserved using RNAlater upon sample collection and subsequently extracted from each sample using Qiagen RNeasy plus Mini kits. Illumina stranded mRNA-seq libraries were prepared and sequenced as paired end reads at University of Minnesota Genome Center. Libraries were sequenced across three lanes and pooled together to minimize lane (batch) effects.

RNA-sequencing:

We performed quality control on the sequencing reads using fastp v.0.23.1. Reads that were less than 20 bp long were removed, and at least $\frac{1}{3}$ of each remaining read was required to have a PHRED base quality score above 30 to be kept. Next, reference data was obtained from DictyBase on January 16, 2023, and included a *D. discoideum* reference genome (FASTA), a gene annotation file (GTF), and a Gene Ontology (GO)

annotation file. The GTF file was used by STAR to identify splice junctions during alignment, and was also used to count the number of reads aligned to each specific gene. The reference genome was indexed and reads were aligned to the indexed reference using STAR v.2.7.5c, a splice-aware aligner (Dobin et al., 2013). To process the alignments and check the quality, only reads mapped in proper pairs were included and sorted by read query using SAMtools v.1.3.1 (Li et al., 2009). Read groups were added using SAMtools and subsequently counted using htseq-count v.0.11.2 (Anders et al., 2015). The count table was generated with the -s reverse flag to ensure the stranded libraries were counted in the correct orientation for reads with a minimum alignment quality score of 20. The reverse option denoted that the stranded library preserved strand information by degrading the non-template strand and PCR amplifying only the template cDNA strand during library construction (Srinivasan et al., 2019).

Differential expression analysis:

The count tables were loaded into R v.4.2.2 with supplementary packages ggplot2 v.3.5.5 (Wickham, 2016), RColorBrewer v.1.1-3 (Neuwirth and Brewer, 2014), and dplyr v.1.1.1 (Wickham et al., 2014). Differential expression analysis was performed with DESeq2 v.1.38.3 using a negative binomial generalized linear model (Love et al., 2014). To contextualize the count tables, a metadata table of all the factors in the study was created. Included were sample file name, *D. discoideum* host strain, time collected (control, 90 mpi, 360 mpi, positive), and *Paraburkholderia* type ($\Delta tssH$ or WT) (Noh et al., 2022). Two analyses were performed. First, a pairwise contrast of differential gene expression between the $\Delta tssH$ mutant and WT *P. bonniea* 433. Then, to contrast the

development of infection over time, three pairwise contrasts for each infected time point compared to the control time point were set up. For each contrast, differential expression analysis was performed using Wald tests for significance with a false discovery rate of 0.05. Visualizations were performed to explore differential expression changes. Venny v.2.1.0 was used to generate venn diagrams that visualized overlapping differentially expressed genes (Oliveros, 2007-2015).

GO term enrichment analysis:

GO enrichment analysis was performed on the identified candidate genes from DESeq2 using GOstats v.2.64.0 (Falcon and Gentleman, 2007). Enrichment tests provide possible explanations for the expression variation found in the significantly differentially expressed genes by identifying related system-wide biological processes and functions. To prepare for GO term enrichment, annotations with 'NOT' qualifiers evidence codes, 'ND' (No biological Data available) evidence codes, and annotations lacking a source were filtered out. Lists of up and downregulated genes were constructed, with significant p-values below 0.05. We used GSEABase v.1.60.0 to load the respective gene list, ontology file, and GO annotations (Morgan et al., 2022). We used GOstats to perform a hypergeometric significance test with a p-value cut off of 0.05 to test for enrichment using counts in up and downregulated genes. To visualize the GO term enrichment results, semantic bubble plots were generated with GO-Figure! v.1.0.1 (Reijnders and Waterhouse, 2021) using the GOstats result table. Graphs ranging from 6-60 bubbles were constructed, depending on the number of terms present in the result table.

Results:

Host Fitness:

To characterize how the relationship between host fitness and symbiont infection prevalence differed between *P. bonniea* $\Delta tssH$ and WT, two nonnative *D. discoideum* hosts were exposed to two $\Delta tssH$ and wildtype strain pairs of *P. bonniea* at a range of MOIs. Host fitness was measured as the relative spore counts, and decreased as infection prevalence increased for all combinations (Figure 2). The relative counts were used to indicate the proportion of *D. discoideum* spores that survived an infection compared to the uninfected control. Relative counts between hosts infected with the $\Delta tssH$ mutant and wildtype variants were significantly different for *P. bonniea* 433 ($F = 10.6$, $p = 0.002$) but not significantly different for *P. bonniea* 859 ($F = 0.2$, $p = 0.6$) (Figure 1). Average host fitness (mean of relative spore counts) was not significantly different (Wilcoxon test, $W = 1144$, $p = 0.7135$) and host fitness responses did not change between the $\Delta tssH$ mutant and wildtype. Between the $\Delta tssH$ mutant and wildtype pairs for each strain, we compared how host fitness changed with a unit increase in infection prevalence (slope). We found that this relationship measuring host fitness response was not significantly different between wildtype and $\Delta tssH$ infected hosts ($F_{433} = 1.9$, $p_{433} = 0.2$, $F_{859} = 0.01$, $p_{859} = 0.9$) (Figure 2). However, the average infection prevalence was lower for the $\Delta tssH$ mutant *P. bonniea* across both hosts (Wilcoxon test, $W = 1354.5$, $p = 0.07$). Between the wildtype and mutant $\Delta tssH$ *P. bonniea* infected hosts, there was about a 20% decreased infection prevalence for the knockout for both hosts at the maximum MOI (Figure 2). Although infection prevalence

was different between $\Delta tssH$ and wildtype infected hosts, there was a similar host fitness response due to increasing infection prevalence.

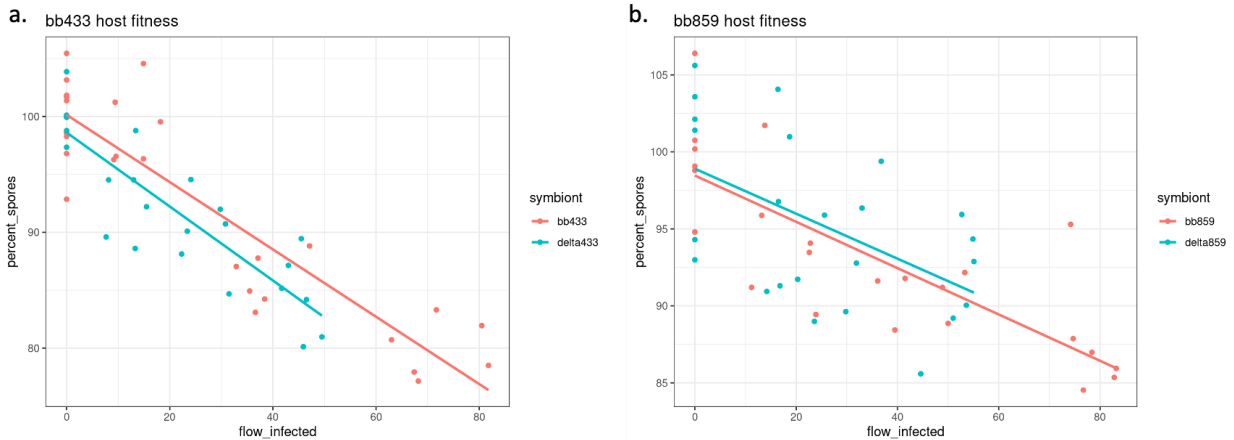


Figure 2: Infection prevalence compared to relative spore production, with host fitness decreasing as infection prevalence increased. The slopes are the change in host fitness with an increase in infection prevalence, which were not significantly different between the $\Delta tssH$ mutant and wildtype pairs for each strain. (a) Host fitness between wildtype (blue) and $\Delta tssH$ (red) *P. bonniea* 433. Wildtype infection prevalence extended to 81.8%, while $\Delta tssH$ infection prevalence extended to 50%. (b) Host fitness between wildtype (blue) and $\Delta tssH$ (red) *P. bonniea* 859. Wildtype infection prevalence extended to 83.4%, while $\Delta tssH$ infection prevalence extended to 54.9%

Horizontal Transmission:

Next, we characterized the relationship between symbiont transmission and initial symbiont infection between $\Delta tssH$ *P. bonniea* and wildtype *P. bonniea*. *D. discoideum* hosts were exposed to amoeba pre-infected with $\Delta tssH$ and wildtype strain pairs of *P. bonniea* during the *D. discoideum* social cycle. We estimated the percentage of newly

infected spores as a measure of horizontal transmission. Infection prevalence is a combination of *P. bonniea*'s ability to infect *D. discoideum* and horizontally transmit infection. Symbiont transmission increased with infection prevalence of pre-infected amoebas ($F_{433} = 196$, $p_{433} = 0$, $F_{859} = 85.8$, $p_{859} = 0$). This positive correlation reflects horizontal transmission, rather than vertical transmission (Ebert, 2013). Increased transmission rates onto previously uninfected hosts may be indicative of better symbiont performance by being able to better spread from host to host. The percent of horizontally transmitted infected spores and infection prevalence in $\Delta tssH$ *P. bonniea* were lower for both hosts ($F_{433} = 36.9$, $p_{433} = 0$, $F_{859} = 24.4$, $p_{433} = 0$) (Figure 3). This large reduction of a horizontally transmitted population also reflects a reduced ability to infect from within a host with the $\Delta tssH$ mutants, as overall infection prevalence was lower than in the first social cycle as seen in the host fitness assay (Figure 2, Figure 3). $\Delta tssH$ variant symbionts had a shallower slope as well as reduced infection prevalence compared to their respective wildtype counterparts ($F_{433} = 14.6$, $p_{433} = 0.0006$, $F_{859} = 69.9$, $p_{859} = 0$) (Figure 3).

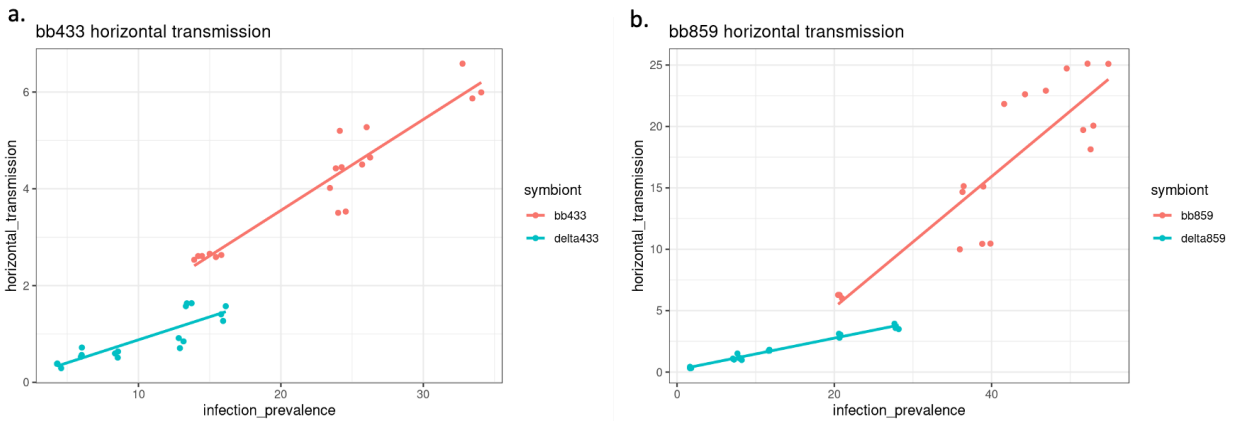


Figure 3: Infection prevalence compared to horizontal transmission rates. (a) Horizontal transmission between wildtype (blue) and $\Delta tssH$ (red) *P. bonniea* 433. (b) a) Horizontal transmission between wildtype (blue) and $\Delta tssH$ (red) *P. bonniea* 859.

RNA-seq

ΔtssH mutant vs wildtype:

We tested for differential gene expression in two host strains infected with $\Delta tssH$ *P. bonniea* 433 compared to wildtype *P. bonniea* 433 samples in order to evaluate transcriptional differences during the first six hours of infection. Out of 8490 aligned genes, none were found to be significantly differentially expressed at a false discovery rate (FDR) of 0.1. This was expected, as reflected by our PCA visualization and host fitness assays, which failed to find a significant difference between $\Delta tssH$ and wildtype variations between infection prevalence and relative spore counts (Figure 2, Figure 4).

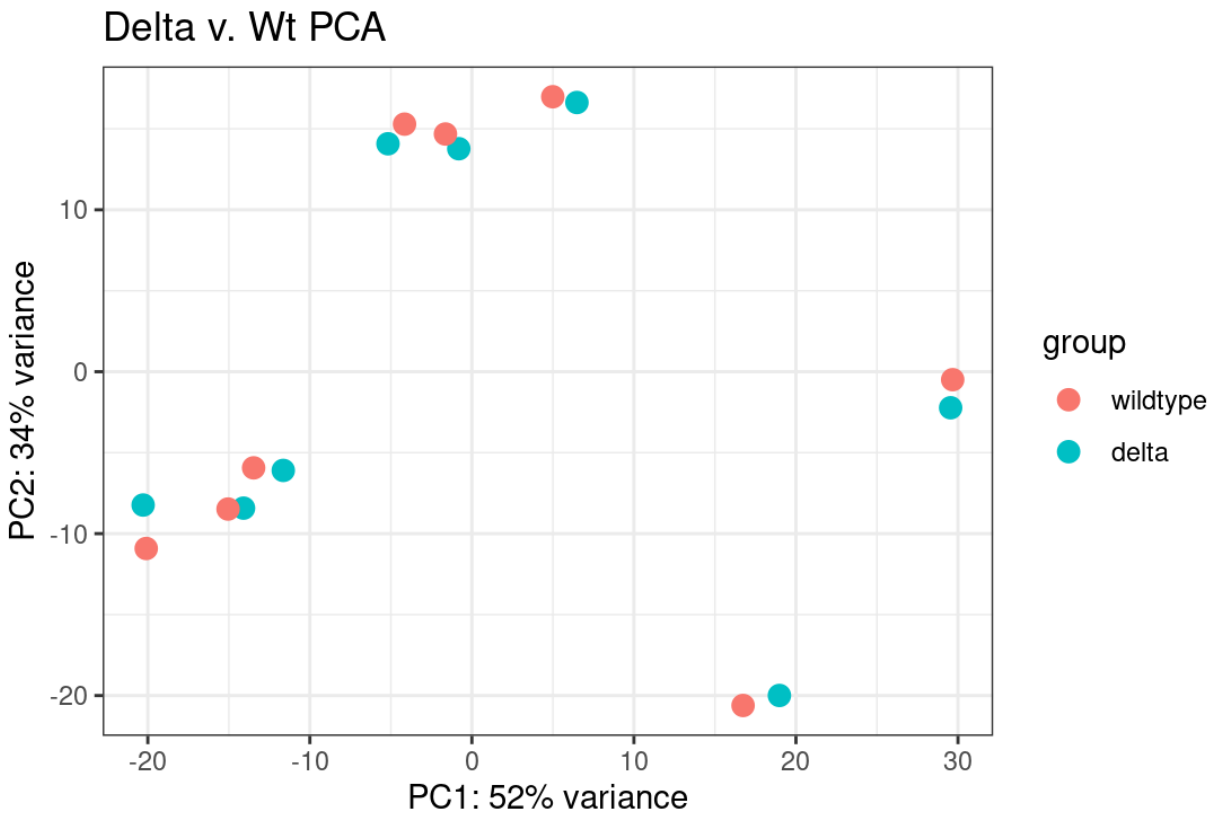


Figure 4: PCA plot displaying negative controls and wildtype and $\Delta tssH$ *P. bonniea* 433 infected *D. discoideum* hosts collected at 90 mpi, 360 mpi, and positive controls. Variation along the first 2 principal components are displayed.

Time series:

We tested for differential gene expression at 90 mpi, 360 mpi, and a long term infection (positive controls; approximately 2250 mpi) for WT and $\Delta tssH$ *P. bonniea* 433 infected hosts in order to evaluate infection progression and transcriptional differences during a new infection. To accomplish this, we grouped the WT and $\Delta tssH$ infected hosts and compared differential expression across time points. Initial visualization displayed a sharp segregation of 360 time points from all other time samples, which was reflected in

the number of differentially expressed genes (Figure 5). Differential expression was computed across pairwise comparisons of each infected time point to negative controls with an applied FDR of 0.05. Out of 8490 genes with minimal levels of expression, 82 (0.97%) were upregulated and 129 (1.5%) were downregulated at 090 mpi, 1519 (18%) were upregulated and 1532 (18%) were downregulated at 360 mpi, and 630 (7.4%) were upregulated and 772 (9.1%) were downregulated for the positive control (Figure 6). The differential expression map for each time point indicates the clear differences at the 360 time point, compared to less defined patterns observed in the other time points is shown (Figure 7). Both up and down regulated differentially expressed genes only share about 1% of genes among all time points as infection progresses, but 10% of upregulated genes were overlapping between 360 mpi and the positive control, and 14% of downregulated genes (Figure 8). We theorize this represents the peak of the infection, where the host has to activate the most genes to respond to the *P. bonniea* infection. In order to gain further insight into the functions and observed patterns of these different differentially expressed genes, GO analysis was performed by grouping the differentially expressed genes into gene ontology groups.

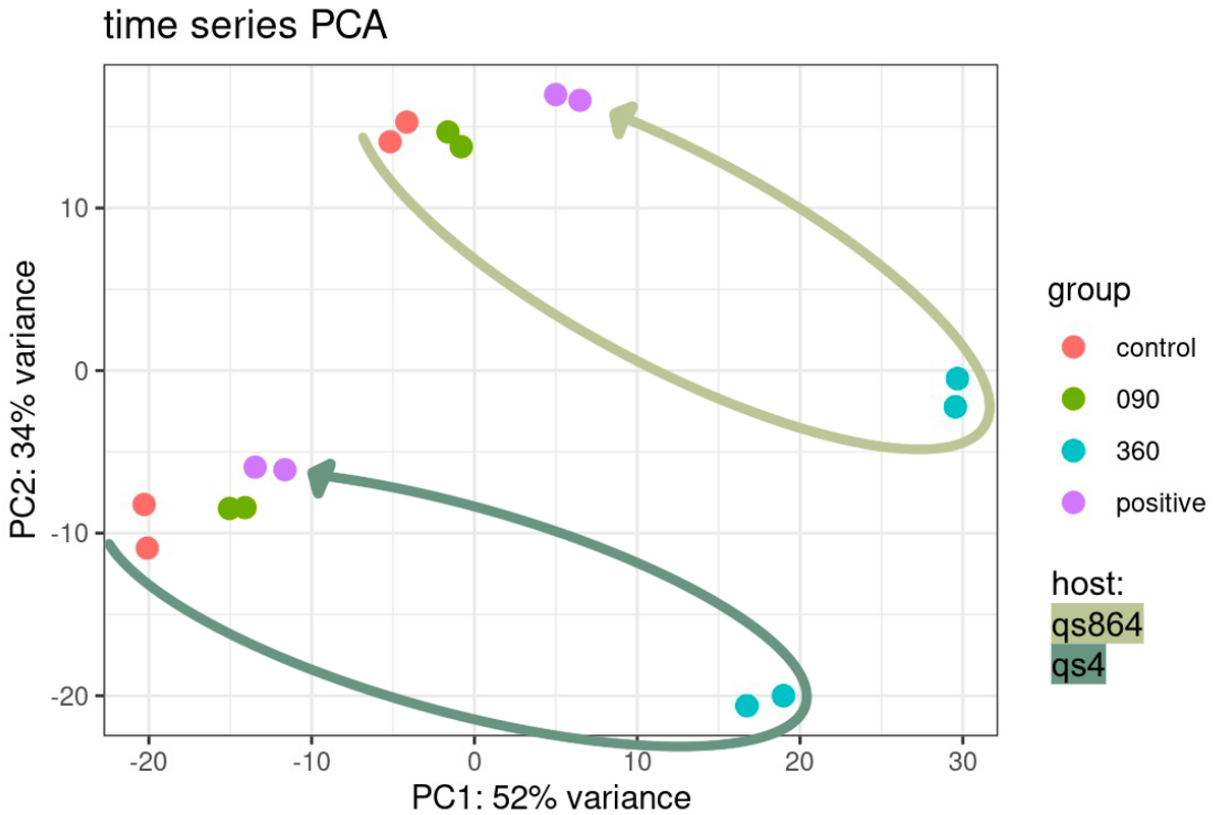


Figure 5: PCA plot displaying negative controls $\Delta tssH$ / wildtype *P. bonniea* 433 infected *D. discoideum* hosts collected at 90 mpi, 360 mpi, and positive controls. In this visualization, WT and $\Delta tssH$ infected hosts were grouped together and compared across time points. Variation along the first 2 principal components are displayed. Arrows show the trajectory of gene expression across time within a host.

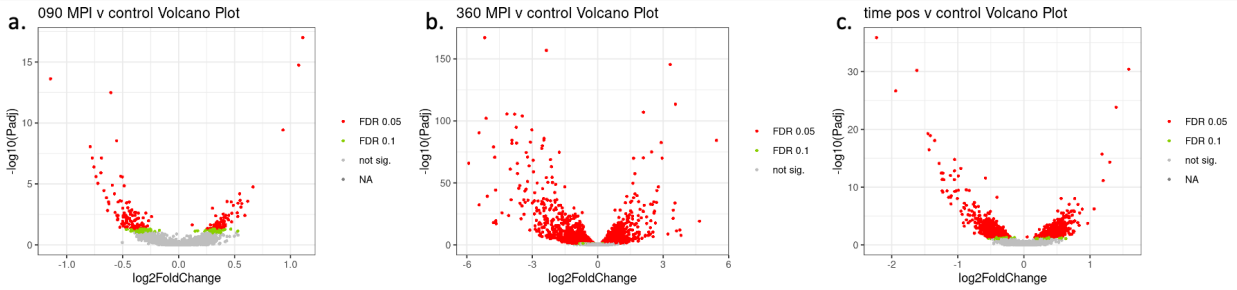


Figure 6: Volcano plot for infected vs uninfected *D. discoideum* for different time points of *P. bonniea* WT and $\Delta tssH$ infection at a FDR of 0.05 and 0.1. Upregulated genes are towards the right, and downregulated genes are towards the left. Statistically significant genes marked in red with a FDR of 0.05, and genes marked in green are significant with a FDR of 0.1. (a) 090 mpi versus negative control (b) 360 mpi versus negative control (c) positive control mpi versus negative control.

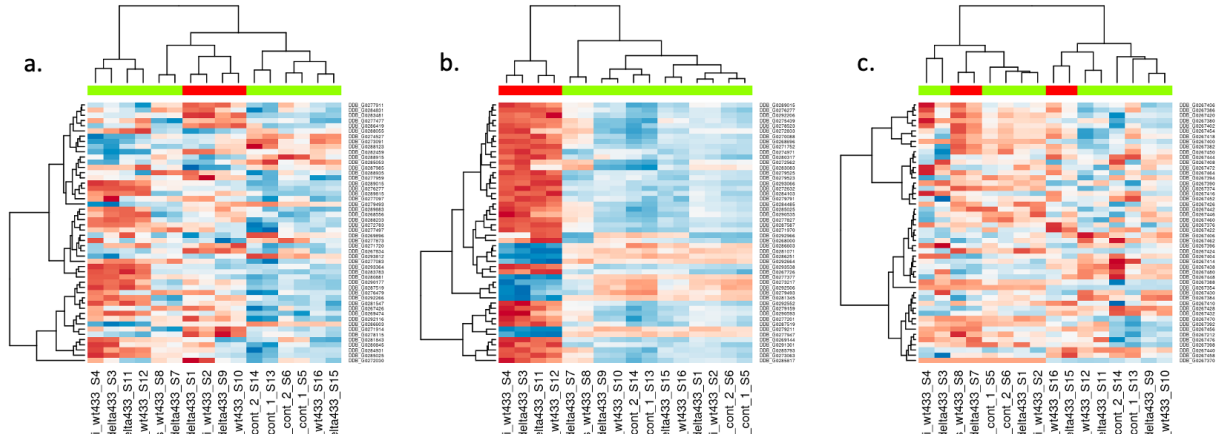


Figure 7: Differential expression heat map for infected vs uninfected *D. discoideum* for different time points. Red indicates upregulated genes, while blue represents downregulated genes in the infected sample compared to the control. The red bar indicates the infected *D. discoideum* samples collected at the time point of choice. (a) 090 mpi versus negative control (b) 360 mpi versus negative control (c) positive control mpi versus negative control.

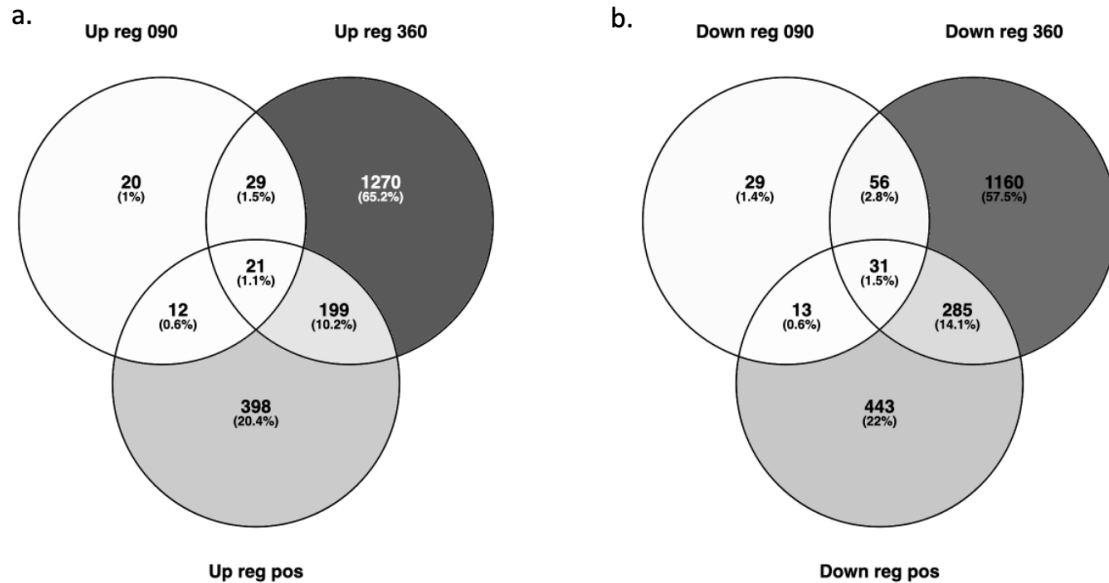


Figure 8. Venn diagrams displaying overlapping differentially expressed genes between pairwise comparisons of an infected *D. discoideum* host versus control at different time points. The darker the section, the higher the percentage of genes in that category (a). Upregulated differentially expressed genes. (b) Downregulated differentially expressed genes.

By performing GO pathway enrichment and semantic analysis on up and downregulated differentially expressed genes at each time point, we were able to better characterize the functions of these genes. At 090 mpi, no distinct clusters of GO terms were seen due to the low number of differentially expressed genes. The upregulated functions focused on aggregation and potassium ion transport and stress responses in our infected host cells, and the downregulated functions involved metabolic processes (Figure 9). The largest number of up and downregulated GO functional groups were found at 360 mpi out of all time points. Major upregulated functional clusters encompass

amino acid metabolism, transmembrane transport and phagocytosis, cytoskeleton regulation, and signal transduction (Figure 10a). Many of the upregulated GO terms involved actin filaments, which are a network that provides mechanical support, determines cell shape, and regulates movement on the cell surface, allowing cells to migrate, engulf particles, and divide (Cooper, 2000). Additionally, both the tricarboxylic acid (TCA) metabolic processes and TCA cycle were downregulated at 090 mpi, but upregulated at 360 mpi. The TCA cycle primarily provides NADH which amoeba cells use for ATP synthesis via the electron transport chain. However bacterial pathogens also modulate the host TCA cycle to drive stress tolerance mechanisms through the generation of reactive oxygen species (ROS) (Passalacqua et al., 2016; Thomas et al., 2013). The TCA cycle can produce NADPH oxidase, which are commonly found in “professional phagocytes” such as *D. discoideum*. The phagocyte oxidase has been thought to function by generating reactive oxygen species (ROS) from the electrons in the NADPH. These ROS kill microbes and play a role in the pathogenesis of disease by damaging normal tissues (Cross and Segal, 2004; Segal, 2008). Other key trends were energy production, nucleotide biosynthesis, and phagocytosis. The upregulation of phagocytosis is interesting, as that is *D. discoideum*'s main defense against invading pathogens, indicating an increasing host response to infection (Dunn et al., 2017; Sillo et al., 2008). The GO groups in the downregulated semantic bubble plot for 360 mpi were generally more spread out, with one cluster focused on cellular assembly and another cellular replication and division (Figure 10b). Overall, many functions related to the cell cycle and cellular division were downregulated at 360 mpi, which may be a result of the hosts undergoing cell division and mitosis earlier in the time series.

For a longer term infection, modeled by the positive control data, there were intermediate numbers of enriched GO terms. In upregulated terms, signal transduction pathways for communication and transport functions were clustered together (Figure 11a). For downregulated terms, the terms covered metabolic and biosynthesis pathways, immune response and apoptosis (Figure 11b). Especially of note, reactive oxygen species metabolic functions were downregulated (Figure 11b), as a direct contrast to the TCA cycle being upregulated at 360 mpi (Figure 10a).

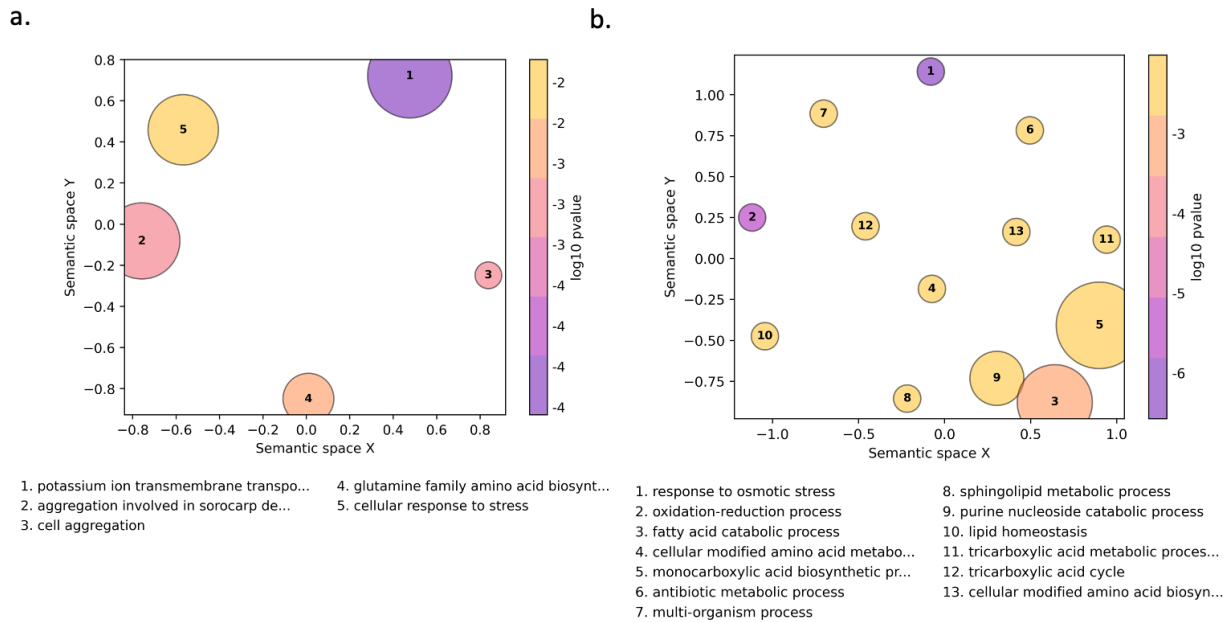


Figure 9: GO semantic bubble plot for differentially expressed genes contrasting *D. discoideum* infected with *P. bonniea* 433 Δ tssH / WT at 090 mpi vs uninfected *D. discoideum*. Each bubble represents an enriched functional category, the bubble size represents gene counts, and the color represents the p-value. The semantic space x and y axis are constructed so semantically similar GO terms are also closer in the plot. Relative positioning of the plotted terms summarizes the key functional information (a) 19 upregulated GO terms were used to create 5 functional groupings. (b) 22 downregulated GO terms were used to create 13 functional groupings.

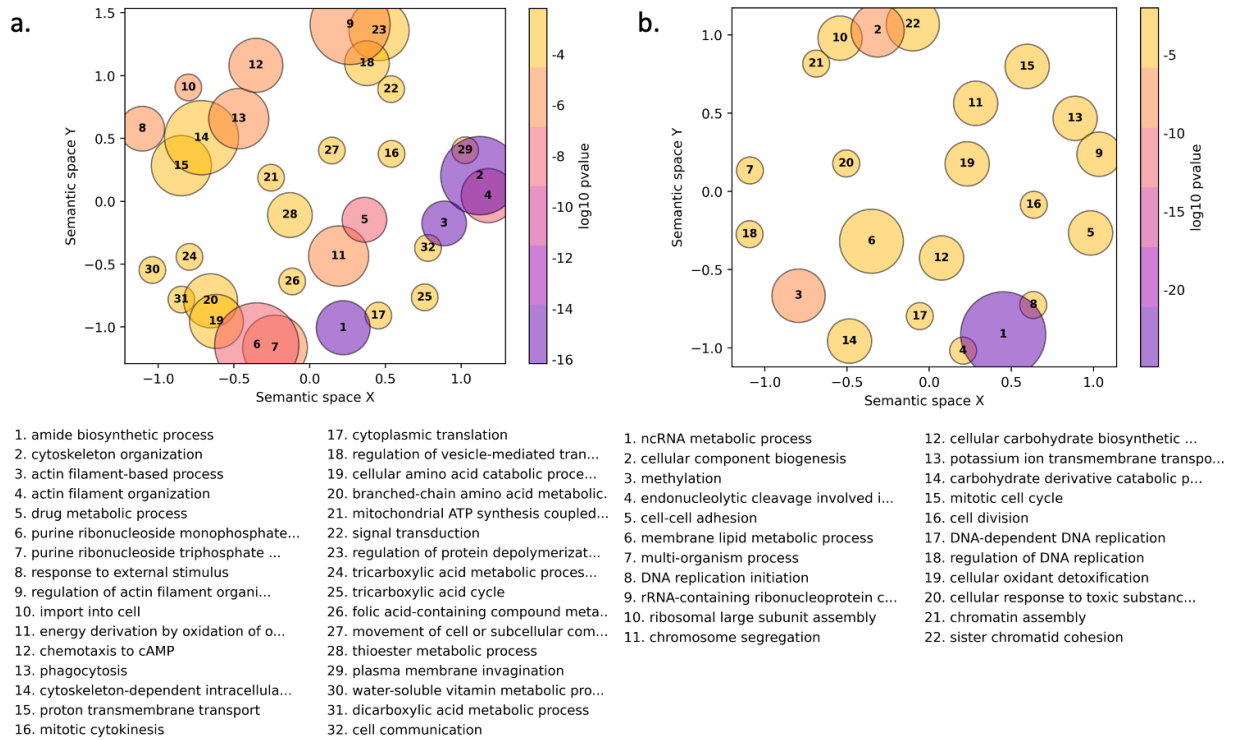


Figure 10: GO semantic bubble plot for differentially expressed genes contrasting *D. discoideum* infected with *P. bonniea* 433 Δ tssH / WT at 360 mpi vs uninfected *D. discoideum*. Each bubble represents an enriched functional category, the bubble size represents gene counts, and the color represents the p-value. The semantic space x and y axis are constructed so semantically similar GO terms are also closer in the plot. Relative positioning of the plotted terms summarizes the key functional information (a) 102 upregulated GO terms were used to create 32 functional groupings. (b) 56 downregulated GO terms were used to create 22 functional groupings.

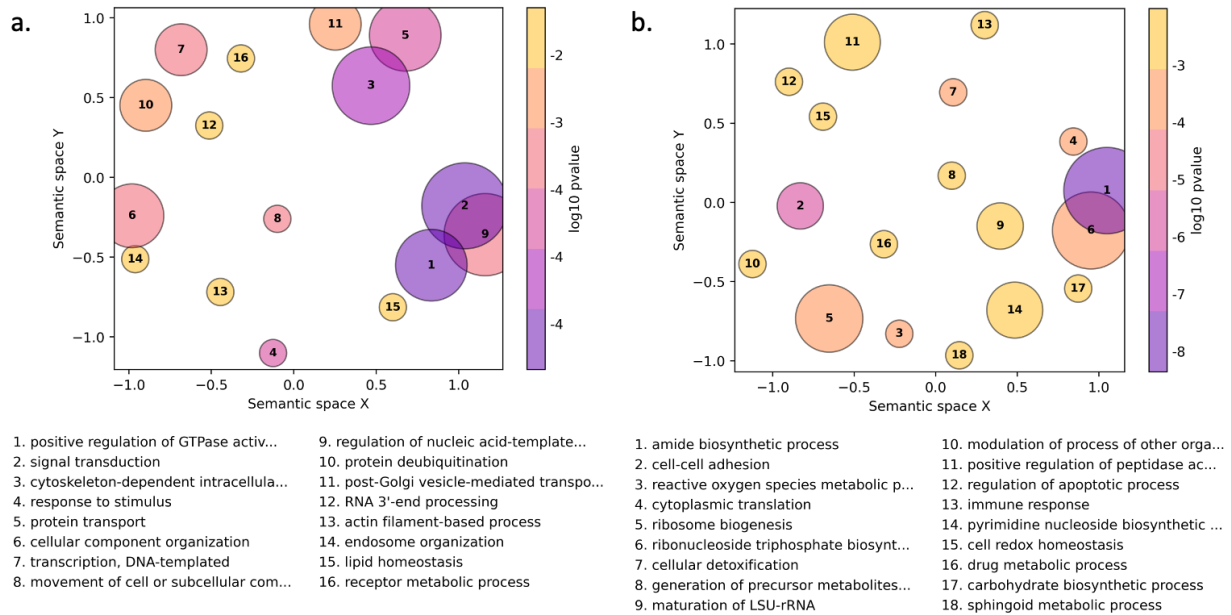


Figure 11: GO semantic bubble plot for differentially expressed genes contrasting *D. discoideum* infected with *P. bonniea* 433 $\Delta tssH$ / WT at a long term infection (2250 mpi) vs uninfected *D. discoideum*. Each bubble represents an enriched functional category, the bubble size represents gene counts, and the color represents the p-value. The semantic space x and y axis are constructed so semantically similar GO terms are also closer in the plot. Relative positioning of the plotted terms summarizes the key functional information (a) 42 upregulated GO terms were used to create 16 functional groupings.(b) 49 downregulated GO terms were used to create 18 functional groupings.

Discussion:

The contractile injection system of the T6SS is a key factor for virulence in many gram negative bacteria to deliver effectors directly into eukaryotic host cell cytosols or other bacteria (Chen et al., 2011; Francis et al., 2002; Lennings, 2018; Taylor et al., 2018). By deleting the *tssH* ATPase gene in the T6SS, we created a dysfunctional T6SS by incapacitating sheath retraction (Förster et al., 2014; Gallique et al., 2017). Comparing the $\Delta tssH$ gene and wildtype, we were able to characterize how a dysfunctional T6SS affected *P. bonniea*'s ability to form a symbiotic relationship with *D. discoideum*.

Host fitness results affirmed that increasing infection prevalence does have a negative effect on host fitness. However, when comparing $\Delta tssH$ and wildtype *P. bonniea* variants, no differences in how host fitness changed as infection prevalence increased was found between them, although there was a significant difference in infection prevalence. The lack of difference in host fitness outcomes was supported by differential gene expression analysis of *D. discoideum* infected by $\Delta tssH$ or wildtype *P. bonniea* 433 during the first six hours of infection. There were no differentially expressed genes found when testing $\Delta tssH$ versus wildtype samples at each time point.

Wildtype *P. bonniea* had significantly higher rates of horizontal transmission compared to $\Delta tssH$. When collecting preliminary data for the RNA-sequencing experiment, *D. discoideum* amoebas had similar infection rates in the first 6 hours post infection, regardless if the hosts were infected with the $\Delta tssH$ or wildtype variant. This matches the host fitness response, where the initial infection levels were not impacted by the

tssH deletion. Thus, the difference in infection prevalence range was most likely due to reduced transmission that occurs after the initial infection over the course of 5-7 days. In *B. pseudomallei*, the T6SS is only activated after the bacteria enters the host cells, while the T3SS is activated immediately after bacteria encounter host cells (Chen et al., 2011). Thus, it makes sense that host fitness was not significantly affected by the deletion, as that was when *P. bonniea* initially entered the host cell, but symbiont transmission from one host to another is reduced in $\Delta tssH$. However, expression levels of both T3SS and T6SS genes increase rapidly upon infection, suggesting that these secretion systems are necessary for bacterial survival, intracellular growth, and replication immediately after infection (Chen et al., 2011).

Although there were no differences in differential expression between $\Delta tssH$ and wildtype induced host responses, the RNA-seq time series provided insight into the infection as a whole. When comparing differential gene expression at various time points during the first 6 hours of infection, we were better able to characterize *D. discoideum*'s host response and development to infection. At 090 minutes, there were not many differentially expressed genes compared to the control, which we hypothesize indicated that the infection was not at full force yet and just developing. The upregulated genes focused on aggregation and some transport and stress responses, and the downregulated functions involved metabolic processes. Particularly, potassium ion transmembrane transport was found to be upregulated, which play important roles in activating immune cell function and defense. Potassium is also a significant factor on the symbiont side, as potassium transport has been shown to directly modulate

virulence gene expression, antimicrobial resistance, and biofilm formation in bacteria (Do and Gries, 2021). Osmotic stress was one downregulated response, which is important for limiting the growth of bacteria. Regular structure and metabolism of bacterial cells are maintained through osmosis, so rapid changes caused by osmotic shock may lead to membrane instability and cell death (Sochocka and Boratyński, 2011). Antibiotic metabolic processes and sphingolipid metabolism were also downregulated, which regulate major cellular processes such as apoptosis, proliferation, and senescence (Merrill Jr, 2011). Prevention of defense responses such as apoptosis may provide a survival advantage because it enables the bacteria to replicate inside host cells. These bacterial-mediated responses indicate how *D. discoideum* is adapting to an initial infection by reducing its hostile defenses, allowing an eventual persistent relationship (Faherty and Maurelli, 2008). Additionally, less energy is accessed as many energy-related functions are downregulated like fatty acid catabolism, amino acid metabolism, nucleic acid metabolism, and the TCA cycle, which indicates a host response against infection via nutrient supply (Berry et al., 1954; LibreTexts, 2022; Sánchez-García et al., 2021).

At 360 mpi, *D. discoideum* had the most drastic response to infection with the most number of significant differentially expressed genes between the infected and control samples. This may indicate the most active time of infection. Key upregulated groups include actin filaments, nucleotide biosynthesis, TCA cycle metabolites, phagocytosis, and transmembrane transport. Multiple actin filaments functions were upregulated, which are targeted by bacterial pathogens and are central for motility to shape

movement, phagocytosis and intracellular trafficking during infection as intracellular structural support (Choe and Welch, 2016; Cooper, 2000). Nucleotide biosynthesis is essential for the survival and virulence of pathogenic bacterial species, and nucleotide metabolism regulators are key for production of virulence factors (Goncheva et al., 2022; Kilstrup et al., 2005). Additionally, TCA related pathways and metabolites were upregulated, in contrast to being downregulated at 090 mpi. This difference could be attributed to the broad function of TCA metabolites in both host and bacterial mechanisms during invasion, acting to produce NADH for ATP synthesis and energy generation (Thomas et al., 2013). Additionally, the TCA cycle is involved with the production of ROS through NADPH oxidase. These ROS kill phagocytosed microbes, but also subject host cells to oxidative stress (Spooner and Yilmaz, 2011). Other key upregulated processes include phagocytosis, which when paired with the TCA cycle, subjects pathogens to oxidative and nitrosative stress, and act as *D. discoideum*'s main defense mechanism (Fang, 2016; Sillo et al., 2008)). In the downregulated enriched GO terms, most are related to the cell cycle and cell division of *D. discoideum*. Many bacterial cells have mechanisms to stall host cell division, which may inhibit early cell death of infected cells, allowing the cells to evade immune defenses and cellular integrity checkpoints and continue the infection (Bagga and Buchard, 2014; Burby and Simmons, 2020). Additionally, when running a pilot time series experiment, cell division occurred around the 240 mpi mark, which may lead to downregulation of cell division functions, as it has been completed.

During the long-term infection, there were intermediate numbers of enriched GO terms compared to the other time points. We attribute this decrease from the 360 mpi to a stabilized infection, which leads to *Paraburkholderia*'s ability to sustain and persistently infect *D. discoideum* by adapting the host environment to better suit bacterial presence (Haselkorn et al., 2019). In contrast to the previous time point, where many replication-based pathways were downregulated, many protein synthesis processes are upregulated, such as RNA 3' end processing, protein deubiquitination, and transcription (He, 2016; Kumar, 2019). Additionally, structural elements and transmembrane transport were also upregulated, indicating re-stabilization of host barriers and immune response. (Dunn et al., 2017). Contrasting the 360 mpi upregulated genes, amide biosynthetic processes and other nucleotide and metabolic biosynthetic processes are downregulated during a long-term infection. This could be due to a stabilized infection, where the most severe responses have been eliminated and an equilibrium infection has been reached. Additionally, there was downregulation of many cellular defense genes associated with infection and immune responses, such as metabolic processes of ROS, indicating that the infection is no longer considered an immediate threat, allowing a persistent symbiotic relationship between *D. discoideum* and *P. bonniea*.

To explore the significant findings of the horizontal transmission results, future work could include looking at differential gene expression in the horizontal transmission assay. To accomplish this, we could perform cell sorting when running flow cytometry on the horizontal transmission results. By sorting the cells receiving horizontally transmission of *P. bonniea*, we could extract and sequence their transcripts using

single-cell RNA sequencing. This would allow us to gain further insight onto the function of the T6SS as the bacteria exits from the host cell, to see what host functions are impacted.

Conclusion:

The persistent *D. discoideum* and *Paraburkholderia* symbiotic relationship allows us to investigate the effects of the T6SS known as a key factor for virulence. Although some phenotypic differences were observed between $\Delta tssH$ variants with the *tssH*-ATPase gene knockout within the T6SS and wildtype *P. bonniea* infected *D. discoideum* hosts, their impact on how host fitness changed as infection prevalence increased was not different between the mutant and wildtype. This was also reflected in our RNA-sequencing data, where there were no differentially expressed genes between them. By collecting transcripts from 090 mpi, 360 mpi, and long term infection, we were to characterize the development of an infection, which can be used in future studies for understanding T6SS. However, significant differences were observed between the variants during horizontal transmission. Thus, the T6SS may be closely involved with virulence after the bacteria has entered the cell, rather than immediately upon encountering the host.

Citations:

1. Alteri, CJ, Mobley, HL. 2016. The versatile type VI secretion system. *Virulence Mechanisms of Bacterial Pathogens*, 337-356.
2. Anders, S, Pyl, P T, and Huber, W. 2015. HTSeq—a Python framework to work with high-throughput sequencing data. *bioinformatics*, 31(2), 166-169.
3. Bagga, S, Bouchard, MJ. 2014. Cell cycle regulation during viral infection. *Cell Cycle Control: Mechanisms and Protocols*, 165-227.
4. Berry, LJ, Merritt, P, Mitchell, RB. 1954. The Relation of the Tricarboxylic Acid Cycle to Bacterial Infection: III. Comparison of Survival Time of Mice Infected with Different Pathogens and Given Krebs Cycle Inhibitors and Intermediates. *The Journal of Infectious Diseases*, 144-151.
5. Bozzaro S, Eichinger L. 2011. The professional phagocyte *Dictyostelium discoideum* as a model host for bacterial pathogens. *Curr Drug Targets* 12:942–954. doi: 10.2174/138945011795677782.
6. Brock DA, Douglas TE, Queller DC, Strassmann JE. 2011. Primitive agriculture in a social amoeba. *Nature* 469:393–396. doi: 10.1038/nature09668.
7. Brock DA, Noh S, Hubert ANM, Haselkorn TS, DiSalvo S, Suess MK, Bradley AS, Tavakoli-Nezhad M, Geist KS, Queller DC, Strassmann JE. 2020. Endosymbiotic adaptations in three new bacterial species associated with *Dictyostelium discoideum*: *Paraburkholderia agricolaris* sp. nov., *Paraburkholderia hayleyella* sp. nov., and *Paraburkholderia bonniea* sp. nov. *PeerJ* 8:e9151. doi: 10.7717/peerj.9151.

8. Burby, PE, Simmons, LA. 2020. Regulation of cell division in bacteria by monitoring genome integrity and DNA replication status. *Journal of bacteriology*, 202(2), e00408-19.
9. Burtnick MN, Brett PJ, Harding SV, Ngugi SA, Ribot WJ, Chantratita N, Scorpio A, Milne TS, Dean RE, Fritz DL, Peacock SJ, Prior JL, Atkins TP, DeShazer D. 2011. The cluster 1 type VI secretion system is a major virulence determinant in *Burkholderia pseudomallei*. *Infect Immun* 79:1512–1525.
10. Camacho, C, Coulouris, G, Avagyan, V, Ma, N, Papadopoulos, J, BealerK, MT. 2009. BLAST+: architecture and applications. *BMC Bioinform* 10:42
11. Cascales, E, and Cambillau, C. 2012. Structural biology of type VI secretion systems. *Philosophical Transactions of the Royal Society B: Biological Sciences*, 367(1592), 1102-1111.
12. Chen, G, Zhuchenko, O, Kuspa, A. 2007. Immune-like phagocyte activity in the social amoeba. *Science* 317, 678–681.
13. Chen, Y, Wong, J, Sun, GW, Liu, Y, Tan, GYG, Gan, YH. 2011. Regulation of type VI secretion system during *Burkholderia pseudomallei* infection. *Infection and immunity*, 79(8), 3064-3073.
14. Choe, JE, Welch, MD. 2016. Actin-based motility of bacterial pathogens: mechanistic diversity and its impact on virulence. *FEMS Pathogens and Disease*, 74(8), ftw099.
15. Cooper GM. *The Cell: A Molecular Approach*. 2000 2nd edition. Sunderland (MA): Sinauer Associates; 2000. Structure and Organization of Actin Filaments. Available from: <https://www.ncbi.nlm.nih.gov/books/NBK9908/>

16. Cross, AR, Segal, AW. 2004. The NADPH oxidase of professional phagocytes—prototype of the NOX electron transport chain systems. *Biochimica et Biophysica Acta (BBA)-Bioenergetics*, 1657(1), 1-22.
17. Deshazer D, Brett PJ, Woods DE: The type II O-antigenic polysaccharide moiety of *Burkholderia pseudomallei* lipopolysaccharide is required for serum resistance and virulence. *Molecular Microbiology*. 1998, 30: 1081-1100.
10.1046/j.1365-2958.1998.01139.x
18. Deshazer D, Waag DM, Fritz DL, Woods DE: Identification of a *Burkholderia mallei* polysaccharide gene cluster by subtractive hybridization and demonstration that the encoded capsule is an essential virulence determinant. *Microbial Pathogenesis*. 2001, 30: 253-269. 10.1006/mpat.2000.0430.
19. DiSalvo S, Haselkorn TS, Bashir U, Jimenez D, Brock DA, Queller DC, Strassmann JE. 2015. *Burkholderia* bacteria infectiousy induce the proto-farming symbiosis of *Dictyostelium* amoebae and food bacteria. *Proc Natl Acad Sci USA* 112:E5029–E5037.
20. Do, E A, Gries, CM. 2021. Beyond homeostasis: potassium and pathogenesis during bacterial infections. *Infection and Immunity*, 89(7), e00766-20.
21. Dobin, A, Davis, C. A, Schlesinger, F, Drenkow, J, Zaleski, C, Jha, S, Batut, P, Chaisson, M, & Gingeras, T R. 2013. STAR: ultrafast universal RNA-seq aligner. *Bioinformatics (Oxford, England)*, 29(1), 15–21.
<https://doi.org/10.1093/bioinformatics/bts635>

22. Dunn JD, Bosmani C, Barisch C, et al. 2017. Eat prey, live: *Dictyostelium discoideum* as a model for cell-autonomous defenses. *Front Immunol* 8:1906. doi: 10.3389/fimmu.2017.01906.
23. Ebert, D. 2013. The epidemiology and evolution of symbionts with mixed-mode transmission. *Annu. Rev. Ecol. Evol. Syst.* 44:623–643.
24. Eisenreich, W, Heesemann, J, Rudel, T, et al. 2013. Metabolic host responses to infection by intracellular bacterial pathogens. *Frontiers in Cellular and Infection Microbiology*. 3. <https://doi.org/10.3389/fcimb.2013.00024>
25. Faherty, CS, Maurelli, AT. 2008. Staying alive: bacterial inhibition of apoptosis during infection. *Trends in microbiology*, 16(4), 173-180.
26. Falcon, S, and Gentleman, R. 2007. Using GOstats to test gene lists for GO term association. *Bioinformatics*, 23(2), 257-258.
27. Fang, FC, Frawley, ER, Tapscott, T, Vázquez-Torres, A. 2016. Bacterial stress responses during host infection. *Cell host & microbe*, 20(2), 133-143.
28. Farinholt, T, Dinh, C, Kuspa, A. 2019. Microbiome management in the social amoeba *Dictyostelium discoideum* compared to humans. *Int. J. Dev. Biol.* 63, 447–450.
29. Fazli, M, Harrison, JJ, Gambino, M, Givskov, M, Tolker-Nielsen, T. 2015. In-frame and unmarked gene deletions in *Burkholderia cenocepacia* via an allelic exchange system compatible with gateway technology. *Applied and environmental microbiology*, 81(11), 3623-3630.
30. Förster, A, Planamente, S, Manoli, E, Lossi, NS, Freemont, PS, & Filloux, A. 2014. Coevolution of the ATPase ClpV, the sheath proteins TssB and TssC, and

the accessory protein TagJ/HsiE1 distinguishes type VI secretion classes. *Journal of Biological Chemistry*, 289(47), 33032-33043.

31. Fox J, Weisberg S. 2019. *An R Companion to Applied Regression*, Third edition. Sage, Thousand Oaks CA.
<https://socialsciences.mcmaster.ca/jfox/Books/Companion/>.
32. Francis, MS, Wolf-Watz, H, Forsberg, Å. 2002. Regulation of type III secretion systems. *Current opinion in microbiology*, 5(2), 166-172.
33. Gallique, M, Bouteiller, M, Merieau, A. 2017. The type VI secretion system: a dynamic system for bacterial communication?. *Frontiers in microbiology*, 8, 1454.
34. Garmory HS, Titball RW. 2004. ATP-binding cassette transporters are targets for the development of antibacterial vaccines and therapies. *Infect Immun* 72:6757–6763.
35. Goncheva, MI, Chin, D, Heinrichs, DE. 2022. Nucleotide biosynthesis: the base of bacterial pathogenesis. *Trends in Microbiology*, 30(8), 793-804.
36. Harland DN, Dassa E, Titball RW, Brown KA, Atkins HS. 2007. ATP-binding cassette systems in *Burkholderia pseudomallei* and *Burkholderia mallei*. *BMC Genomics* 8:83.
37. Haselkorn TS, DiSalvo S, Miller JW, Bashir U, Brock DA, Queller DC, Strassmann JE. 2019. The specificity of *Burkholderia* symbionts in the social amoeba farming symbiosis: prevalence, species, genetic and phenotypic diversity. *Mol Ecol* 28:847–862. doi: 10.1111/mec.14982.

38. He, M, Zhou, Z, Shah, AA, Zou, H, Tao, J, Chen, Q, Wan, Y. 2016. The emerging role of deubiquitinating enzymes in genomic integrity, diseases, and therapeutics. *Cell & bioscience*, 6(1), 1-15.
39. Kessin, R.H. 2001. *Dictyostelium: Evolution, Cell Biology, and the Development of Multicellularity*; Developmental and Cell Biology Series; Cambridge University Press: Cambridge, UK, ISBN 978-0-521-58364-0.
40. Khojandi, N, Haselkorn, TS, Eschbach, MN, et al. 2019. Intracellular *Burkholderia* Symbionts induce extracellular secondary infections; driving diverse host outcomes that vary by genotype and environment. *ISME J.* 13, 2068–2081.
41. Kilstrup, M, Hammer, K, Ruhdal Jensen, P, Martinussen, J. 2005. Nucleotide metabolism and its control in lactic acid bacteria. *FEMS microbiology reviews*, 29(3), 555-590.
42. Kjellin, J, Pr anting, M, Bach, F, Vaid, R, Edelbroek, B, Li, Z, ..., S oderbom, F. 2019. Investigation of the host transcriptional response to intracellular bacterial infection using *Dictyostelium discoideum* as a host model. *BMC genomics*, 20(1), 1-18.
43. Kumar, A, Clerici, M, Muckenfuss, LM, Passmore, LA, Jinek, M. 2019. Mechanistic insights into mRNA 3'-end processing. *Current Opinion in Structural Biology*, 59, 143-150.
44. Lennings J, West TE, Schwarz S. 2018. The *Burkholderia* type VI secretion system 5: composition, regulation and role in virulence. *Front Microbiol* 9:3339.

45. Li, H, Handsaker, B, Wysoker, A, et al. 2009. The sequence alignment/map format and SAMtools. *Bioinformatics*. 1000 Genome Project Data Processing Subgroup. 25(16), 2078-2079.
46. Libretexts. 2022. Fatty Acid Catabolism. *Biology LibreTexts*, Libretexts. [https://bio.libretexts.org/Courses/University_of_California_Davis/BIS_105%3A__Biomolecules_and_Metabolism_\(Murphy\)/Fatty_Acids/Catabolism#:~:text=Fatty%20acid%20catabolism%20is%20the,free%20fatty%20acids%20and%20glycerols](https://bio.libretexts.org/Courses/University_of_California_Davis/BIS_105%3A__Biomolecules_and_Metabolism_(Murphy)/Fatty_Acids/Catabolism#:~:text=Fatty%20acid%20catabolism%20is%20the,free%20fatty%20acids%20and%20glycerols).
47. Love, MI, Huber, W, Anders, S. 2014. Moderated estimation of fold change and dispersion for RNA-seq data with DESeq2. *Genome biology*, 15(12), 1-21.
48. Merrill Jr, A H. 2011. Sphingolipid and glycosphingolipid metabolic pathways in the era of sphingolipidomics. *Chemical reviews*, 111(10), 6387-6422.
49. Miller JW, Bocke CR, Tresslar AR, Schniepp EM, DiSalvo S. 2020. *Paraburkholderia* symbionts display variable infection patterns that are not predictive of amoeba host outcomes. *Genes* 11:674. doi: 10.3390/genes11060674.
50. Morgan M, Falcon S, Gentleman R. 2022. *GSEABase: Gene set enrichment data structures and methods*. R package version 1.60.0.
51. Navarro-Garcia, F, Ruiz-Perez, F, Cataldi, Á, Larzábal, M. 2019. Type VI secretion system in pathogenic *Escherichia coli*: structure, role in virulence, and acquisition. *Frontiers in microbiology*, 10, 1965.

52. Neuwirth, E, Brewer, RC. 2014. ColorBrewer palettes. R package version, 1, 4.
53. Noh, S, BJ Capodanno, S Xu, MC Hamilton et al. 2022. Reduced and nonreduced genomes in *Paraburkholderia* symbionts of social amoebas. *mSystems* e00562-22
54. Oliveros, J.C. (2007-2015) Venny. An interactive tool for comparing lists with Venn's diagrams. <https://bioinfogp.cnb.csic.es/tools/venny/index.html>
55. 2, KD, Charbonneau, ME, O'riordan, MX. 2016. Bacterial metabolism shapes the host–pathogen interface. *Virulence Mechanisms of Bacterial Pathogens*, 15-41.
56. Peracino, B, Buracco, S, Bozzaro, S. 2013. The Nramp (Slc11) proteins regulate development, resistance to pathogenic bacteria and iron homeostasis in *Dictyostelium discoideum*. *J. Cell Sci.* 126, 301–311.
57. Pietrosiuk, A, Lenherr, ED, Falk, S, Bönemann, G, Kopp, J, Zentgraf, H, ... Mogk, A. 2011. Molecular basis for the unique role of the AAA+ chaperone ClpV in type VI protein secretion. *Journal of Biological Chemistry*, 286(34), 30010-30021.
58. Reckseidler-Zenteno SL, DeVinney R, Woods DE: The capsular polysaccharide of *Burkholderia pseudomallei* contributes to survival in serum by reducing complement factor C3b deposition. *Infect Immun.* 2005, 73: 1106-1115. 10.1128/IAI.73.2.1106-1115.2005.
59. Reijnders, M J, & Waterhouse, R M. 2021. Summary visualizations of gene ontology terms with GO-Figure!. *Frontiers in Bioinformatics*, 6.
60. Sánchez-García, F. J., Pérez-Hernández, C. A., Rodríguez-Murillo, M., & Moreno-Altamirano, M. M. B. (2021). The Role of Tricarboxylic Acid Cycle

Metabolites in Viral Infections. *Frontiers in cellular and infection microbiology*, 11, 725043. <https://doi.org/10.3389/fcimb.2021.725043>

61. Schwarz S, West TE, Boyer F, Chiang W-C, Carl MA, Hood RD, Rohmer L, Tolker-Nielsen T, Skerrett SJ, Mougous JD. 2010. *Burkholderia* type VI secretion systems have distinct roles in eukaryotic and bacterial cell interactions. *PLoS Pathog* 6:e1001068.
62. Segal, AW. 2008. The function of the NADPH oxidase of phagocytes and its relationship to other NOXs in plants, invertebrates, and mammals. *The international journal of biochemistry & cell biology*, 40(4), 604-618.
63. Shalom, G, Shaw, JG, Thomas, MS. 2007. In vivo expression technology identifies a type VI secretion system locus in *Burkholderia pseudomallei* that is induced upon invasion of macrophages. *Microbiology*, 153(8), 2689-2699.
64. Shu L, Zhang B, Queller DC, Strassmann JE. 2018. *Burkholderia* bacteria use chemotaxis to find social amoeba *Dictyostelium discoideum* hosts. 8. *ISME J* 12:1977–1993. doi: 10.1038/s41396-018-0147-4.
65. Sillo, A, Bloomfield, G, Balest, A, et al. 2008. Genome-wide transcriptional changes induced by phagocytosis or growth on bacteria in *Dictyostelium*. *BMC Genomics* 9, 291.
66. Skriwan, C, Fajardo, M, Hägele, S, et al. 2002. Various bacterial pathogens and symbionts infect the amoeba *Dictyostelium discoideum*. *Int. J. Med. Microbiol.* 291, 615–624
67. Sochocka, M, Boratyński, J. 2011. Osmoregulation—an important parameter of bacterial growth. *Advances in Hygiene and Experimental Medicine*, 65, 714-724.

68. Solomon, JM; Isberg, RR. 2000. Growth of *Legionella pneumophila* in *Dictyostelium discoideum*: A novel system for genetic analysis of host–pathogen interactions. *Trends Microbiol.* 8, 478–480.
69. Spooner, R, Yilmaz, Ö. 2011. The role of reactive-oxygen-species in microbial persistence and inflammation. *International journal of molecular sciences*, 12(1), 334-352.
70. Sun GW, Chen Y, Liu Y, Tan G-YG, Ong C, Tan P, Gan Y-H. 2010. Identification of a regulatory cascade controlling Type III Secretion System 3 gene expression in *Burkholderia pseudomallei*. *Mol Microbiol* 76:677–689.
71. Srinivasan, K, Virdee, S, McArthur, A. 2019. Strandedness During cDNA Synthesis, the Stranded Parameter in htseq-count, and Analysis of RNA-Seq Data. *Preprints.org*, 2019030124.
<https://doi.org/10.20944/preprints201903.0124.v1>.
72. Steinert, M. 2011. Pathogen–host interactions in Dictyostelium, Legionella, Mycobacterium and other pathogens. *Semin. Cell Dev. Biol.* 22, 70–76.
73. Taylor, NM, van Raaij, MJ, Leiman, PG. 2018. Contractile injection systems of bacteriophages and related systems. *Molecular microbiology*, 108(1), 6-15.
74. Thewes, S, Soldati, T, Eichinger, L. 2019. Editorial: Amoebae as Host Models to Study the Interaction with Pathogens. *Front. Cell. Infect. Microbiol.* 9.
75. Thomas, VC, Kinkead, LC, Janssen, A, Schaeffer, CR, Woods, KM., Lindgren, JK, Fey, PD. 2013. A dysfunctional tricarboxylic acid cycle enhances fitness of *Staphylococcus epidermidis* during β -lactam stress. *MBio*, 4(4), e00437-13.

76. Vines, JH, King, JS. 2019. The endocytic pathways of *Dictyostelium discoideum*. *Int. J. Dev. Biol.* 63, 461–471.
77. Walk, A, Callahan, J, Srisawangvong, P, et al. 2011. Lipopolysaccharide enhances bactericidal activity in *Dictyostelium discoideum* cells. *Dev. Comp. Immunol.* 35, 850–856.
78. Wickham, H, Francois, R, Henry, L, Müller, K. 2014. dplyr. *In useR! Conference*.
79. Wickham H. 2016. *ggplot2: Elegant Graphics for Data Analysis*. Springer-Verlag New York. ISBN 978-3-319-24277-4, <https://ggplot2.tidyverse.org>.
80. Wollein Waldetoft, K, Råberg, L, Lood, R. 2020. Proliferation and benevolence—A framework for dissecting the mechanisms of microbial virulence and health promotion. *Evolutionary Applications*, 13(5), 879-888.
81. Zoued, A, Brunet, YR, Durand, E, Aschtgen, MS, Logger, L, Douzi, B, ... and Cascales, E. 2014. Architecture and assembly of the Type VI secretion system. *Biochimica et Biophysica Acta (BBA)-Molecular Cell Research*, 1843(8), 1664-1673.